



The Drag of an Elliptical Airfoil at a Reynolds Number of 1000

Sheila Tobing^{1,*}

¹ Faculty of Engineering, University of Indonesia, UI Depok Campus, Depok 16424, Indonesia

ARTICLE INFO

Article history:

Received 17 March 2022

Received in revised form 10 May 2022

Accepted 17 May 2022

Available online 31 May 2022

Keywords:

Elliptical airfoil; bumblebee kinematics; counter-rotating vortices

ABSTRACT

There have been many studies on the mechanisms of unsteady aerodynamics, such as leading-edge vortex (LEV) formation, wing-wake interaction, and spanwise flow. Spanwise flow can only be observed on three-dimensional wing models; however other phenomena such as LEV and wing-wake interaction can be captured using two-dimensional airfoil models. This study focuses on two-dimensional elliptical airfoil because this profile can generate counter-rotating vortices used by insects to generate aerodynamic forces. This research aims to analyze the drag production of two-dimensional elliptical airfoils flapping with bumblebee-inspired kinematics in asymmetrical normal-hovering mode at a typical Reynolds number range of $Re = O(10^3)$. It is found that drag is generated during the downstroke while thrust during the upstroke. It is also found that the creation and shedding of counter-rotating vortices are closely related to the generation of thrust. The results also indicate that asymmetrical strokes can be used in normal hovering to minimize drag or produce thrust.

1. Introduction

There have been many studies on flapping wing flight on two-dimensional (2D) objects such as airfoil [1–4] and three-dimensional objects such as nature-inspired wings [5–9]. These past studies on flapping wing flight have led to the discovery of unsteady aerodynamic mechanisms such as leading-edge vortex (LEV), spanwise flow and wing-wake interaction. Leading-edge vortex is formed by the flow that separates at the wing's leading edge and reattaches before leaving the trailing edge [5, 10]. Spanwise flow is a base-to-tip flow that limits the growth of leading-edge vorticity, and thus stabilizes LEV and delays its separation from the wing surface [5]. Wing-wake interaction causes the rapid change in aerodynamic forces after supination and pronation due to the interaction between wing and vortices shed during the previous flapping cycles [6, 11]. The unsteady aerodynamic mechanism explains why insects are able to fly, including bumblebees that are deemed unfit to fly based on the aerodynamics of stationary wings.

Bumblebees can carry a heavy load with their small wings [12]. A trait that might relate to the unique vortex rings observed on the wings of bumblebees. The vortex ring on each wing of a

* Corresponding author.

E-mail address: sheilatobing1@gmail.com (Sheila Tobing)

<https://doi.org/10.37934/cfdl.14.5.1623>

bumblebee is seen both in the experiments of real free-flying bumblebees [13] and also numerical simulations [14]. The ring vortices were formed due to the shedding of tip and root vortices. Ring vortices are the three-dimensional form of counter-rotating vortices found on two-dimensional airfoils. This work focuses on elliptical airfoil because counter-rotating vortices were observed in the experiments and simulations of this shape unlike other 2D profile like NACA0012 and flat plate [15–17].

Wang [18] numerically studied an elliptical airfoil (2D) hovering under a figure-of-eight motion and captured counter-rotating vortices. It is concluded that counter-rotating vortices can be observed on two-dimensional airfoils. These vortices are not a tip vortex (TiV) product, which is a phenomenon exclusive to three-dimensional (3D) wings. Counter-rotating vortices were also observed by Poelma [19] in their study using a dynamically-scaled wing in mineral oil at Re of 256. In the numerical study at higher Reynolds numbers of 10^4 to 10^6 done by Wei *et al.*, [20] vortex dipoles were also seen in the flow visualization.

Wang [21] highlighted the importance of drag in supporting the weight of insects that utilize inclined stroke planes such as dragonflies and hoverflies. Insects that use a normal-hovering mode (stroke plane angle = $\beta = 0^\circ$) can experience the same benefit of drag by deploying asymmetrical strokes. The current work analyzes the drag production of 2D elliptical airfoils that flap with bumblebee-inspired kinematics in asymmetrical normal-hovering mode.

This paper is a continuation of our previous work on the lift of an elliptical airfoil at a Reynolds Number (Re) of 1000 [22]. Bumblebees typically fly in the Reynolds number range of thousands, $Re = O(10^3)$ [23, 24]. Therefore $Re = 1000$ is used in the earlier and current studies on elliptical airfoils flapping under bumblebee-inspired kinematics.

Our earlier work [22] focuses on the lift of elliptical airfoils that flap with bumblebee-inspired kinematics. This work concludes that the high lift of bumblebee wings is produced during the formation and shedding of counter-rotating vortices. The amount of lift produced are more than sufficient to sustain the bumblebee's weight and additional loads like pollen. Another important conclusion of this study is that a 2D elliptical airfoil can be used to study 3D bumblebee wings with sufficient accuracy. Therefore, the current study on drag uses a 2D elliptical airfoil to learn 3D bumblebee wings that are more complicated and time-consuming to simulate. The aim of this research is to find the relationship between the drag and vortices shed by an elliptical airfoil that flaps like a bumblebee.

2. Validation

The solver validation case is an elliptical airfoil in a normal-hovering mode ($\beta = 0^\circ$) at $Re = \frac{\pi f A_0 c}{\nu}$ of 157 [7]. The airfoil flaps with flapping kinematics comprise translational and rotational motions that are described by (1) and (2) respectively, with B being pitching amplitude, α_0 is starting angle of attack, and f is flapping frequency (Table 1). The elliptical airfoil has a ratio of flapping amplitude to chord ($= A_0/c$) of 2.5 and the ratio of airfoil thickness to chord ($= t/c$) of 0.125. The validation results show a good agreement between the current solver and the reference data (Figure 1). The computational domain, the mesh details, and the analysis of the validation results have been thoroughly explained in [22].

$$[x(t), y(t)] = \frac{A_0}{2} (1 + \cos 2\pi f t) (\cos \beta, \sin \beta) \quad (1)$$

$$\alpha(t) = \alpha_0 + B \sin(2\pi ft + \varphi) \quad (2)$$

Table 1
Geometry and flow condition of the validation case

Variable	Description	Value
A_0	Flapping/translation amplitude	0.04175 m
f	Frequency	1 Hz
B	Pitching amplitude	45°
β	Stroke-plane angle	0°
φ	Phase angle	0°
α_0	Starting angle-of-attack	90°
c	Airfoil chord	0.01670 m
ν	Kinematic viscosity	1.4e-05 (m ² s ⁻¹) (air)

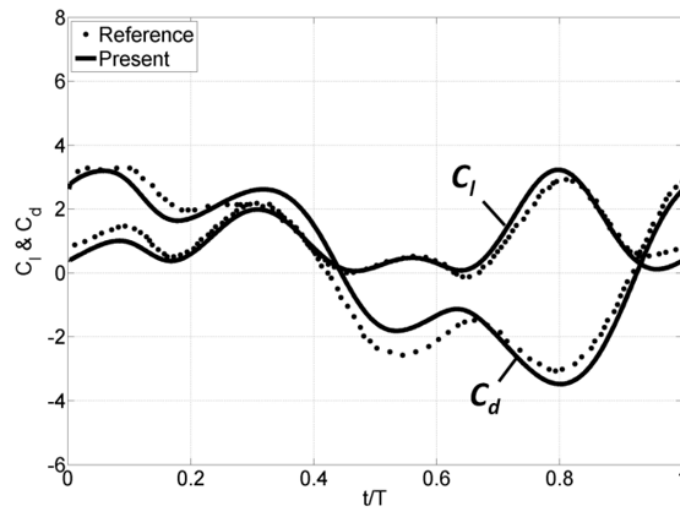


Fig. 1. Validation results [22]

3. Numerical Modeling of Elliptical Airfoil

The elliptical airfoil has the same ratio of translation amplitude to chord ($= A_0/c$) and the ratio of thickness to chord $= (t/c)$ as the validation model. The kinematics of the elliptical airfoil is described in detail in an earlier work [14], with the parameters listed in Table 2. The computational domain consists of 35,442 mixed tetrahedral and triangular cells Figure 2.

Table 2
Kinematics of bumblebee-inspired elliptical airfoil

Variable	Description	Value
c	Airfoil chord	0.01670 m
A_0	Flapping/translation amplitude	0.04175 m
f	Frequency	1 Hz
φ	Phase angle	0°
β	Stroke-plane angle	0°
α_D	Angle-of-attack during downstroke	58.8°
α_U	Angle-of-attack during upstroke	49.3°
ν	Kinematic viscosity	2.19e-06 m ² s ⁻¹

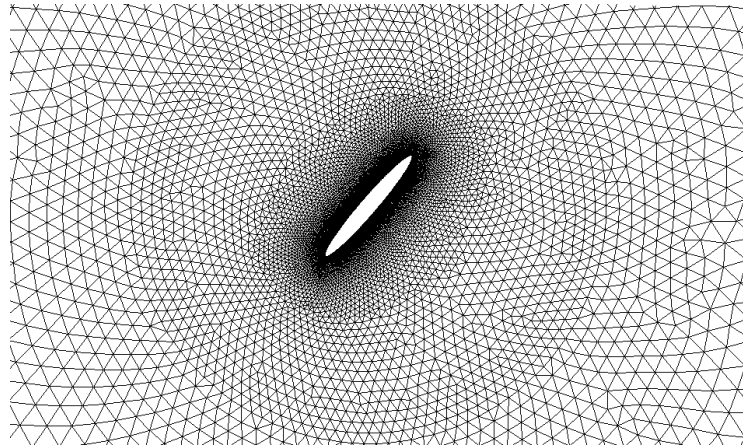


Fig. 2. Computational domain

4. Drag and Thrust at Reynolds Number 1000

A repetitive time history of forces is achieved after 12 flapping cycles/wingbeats (Figure 3). The time-averaged drag coefficient ($\overline{C_d}$) of the 12th cycle is 0.0470. The time history of drag/thrust and the time instances of interests are shown in Figure 3. A positive value of C_d means drag, while a negative one means thrust.

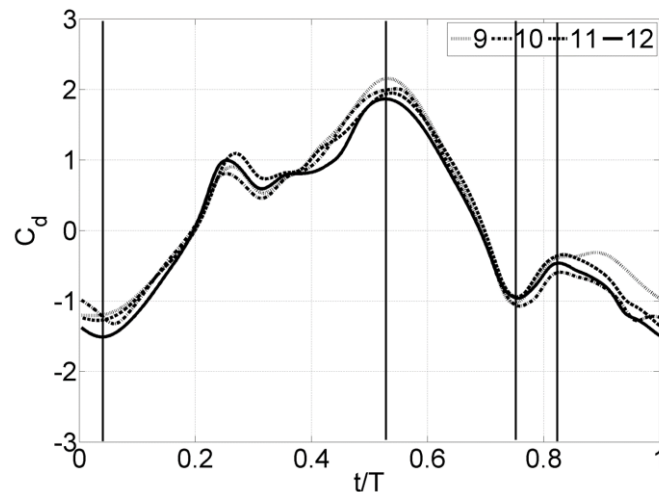
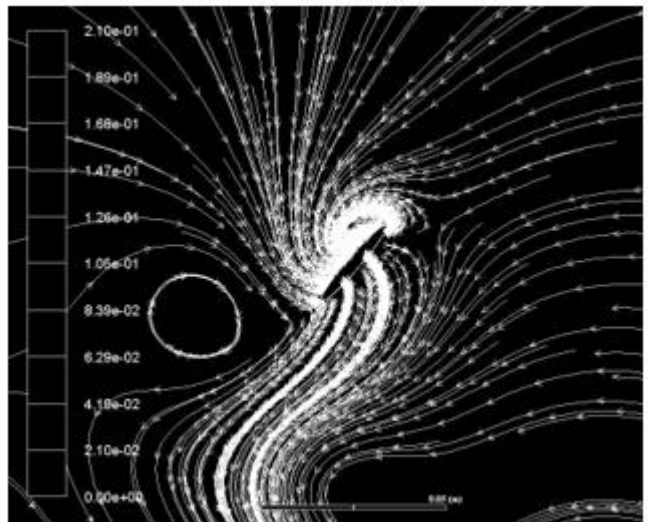
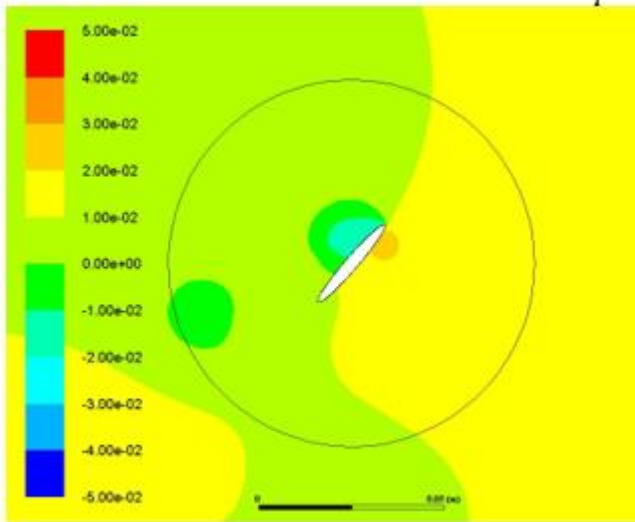
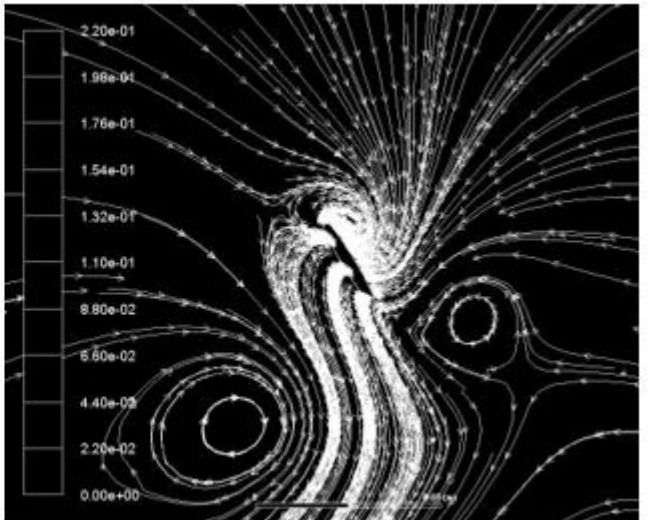
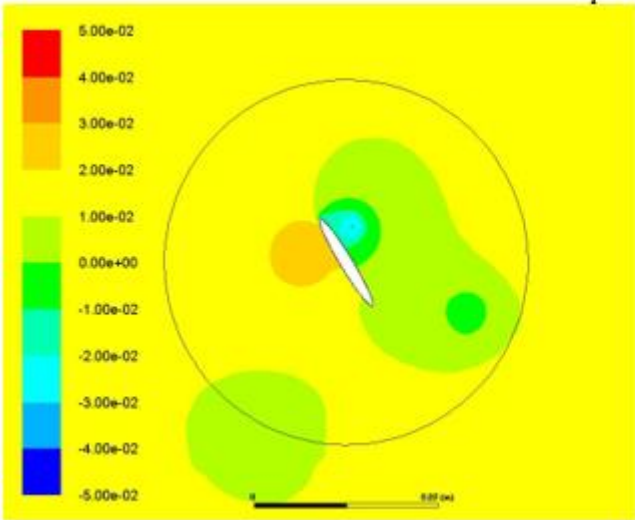


Fig. 3. Time history of the drag coefficient. From left to right are lines marking t/T of 0.04, 0.52, 0.78, and 0.82

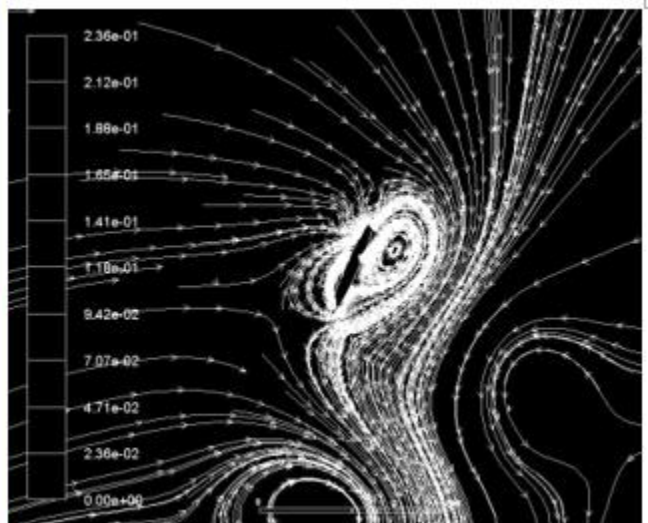
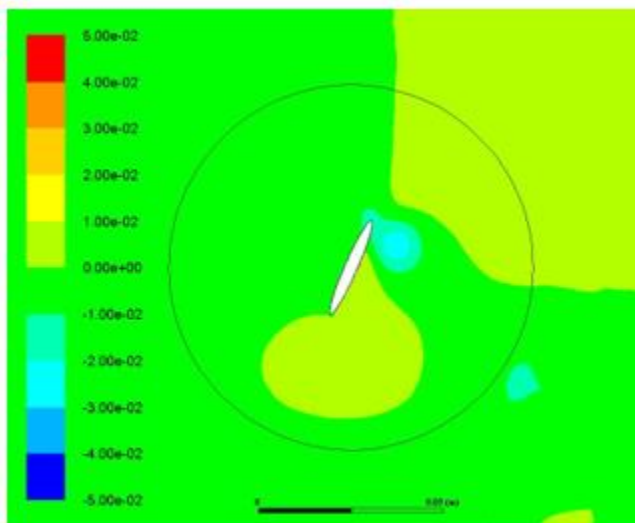
At 0.04 of a cycle, counter-rotating vortices can be seen with a counter-clockwise LEV attached to the airfoil while a clockwise TEV from the previous cycle has been shed (Figure 4). This LEV creates a low-pressure region (blue area) on the upper surface; in combination with the higher pressure (yellow-orange area) on the lower surface, this results in the global maximum of thrust ($C_d = -1.5106$).



$$\frac{t}{T} = 0.04$$



$$\frac{t}{T} = 0.52$$



$$\frac{t}{T} = 0.78$$

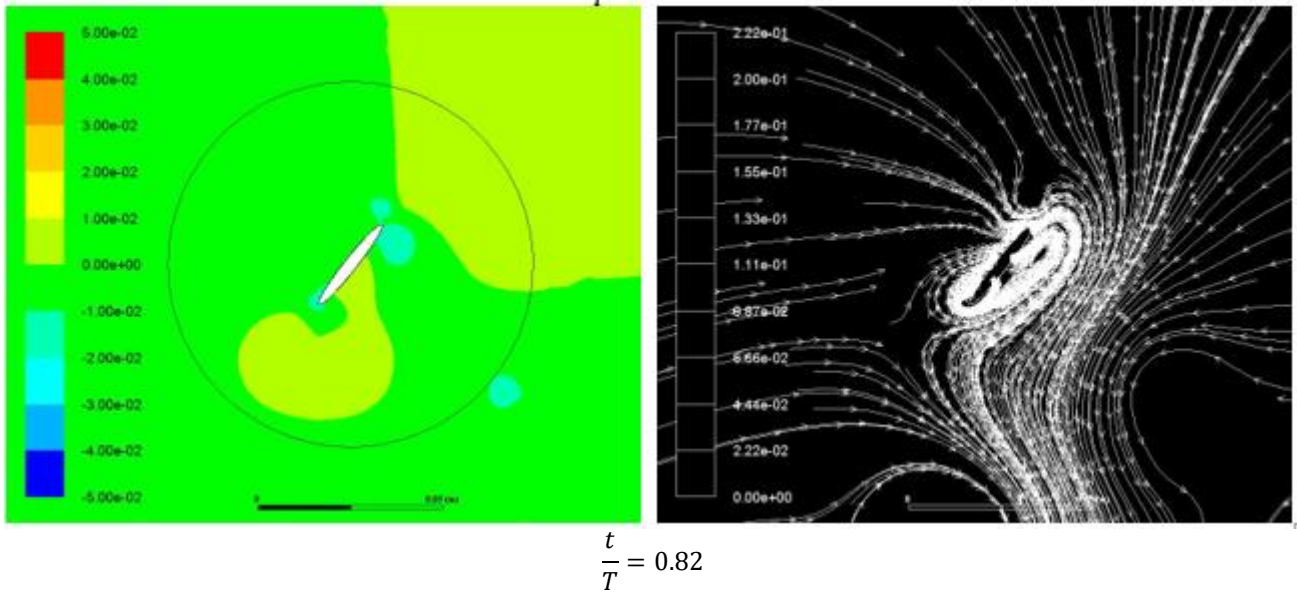


Fig. 4. Flow visualization. Left: contour of static pressure and Right: flow path-lines

At 0.52, a new LEV has grown on the upper surface. This LEV creates a low-pressure region on the corresponding surface, hence the high drag coefficient value (a global maximum of drag, $C_d = 1.8580$). The counter-rotating vortices are visible with the TEV has detached from the airfoil and rotates in a counter-clockwise direction, and the LEV rotates in the opposite direction. This TEV provides extra circulation under the airfoil and "pushes" the flow downward, creating a high lift and a high drag at the time instance.

At 0.78, the airfoil flips, and its TE is exposed to the downward push of the shed TEV. This push creates a higher pressure around the TE, resulting in a force in the x -axis, or thrust is generated (a local maximum, $C_d = -0.8354$). At 0.82, a new TEV is formed and creates a low-pressure region. This region reduces the amount of thrust generated by the airfoil ($C_d = -0.4717$).

At 0.9, the counter-rotating vortices are visible with a counter-clockwise LEV and a clockwise TEV. The airfoil produces negative drag (= thrust) with $C_d = -0.7518$ (Figure 5). The two vortices create a large suction on the left surface of the airfoil that results in a high thrust force. These counter-rotating vortices continue to develop until the end of the cycle. ($C_d = -1.4967$).

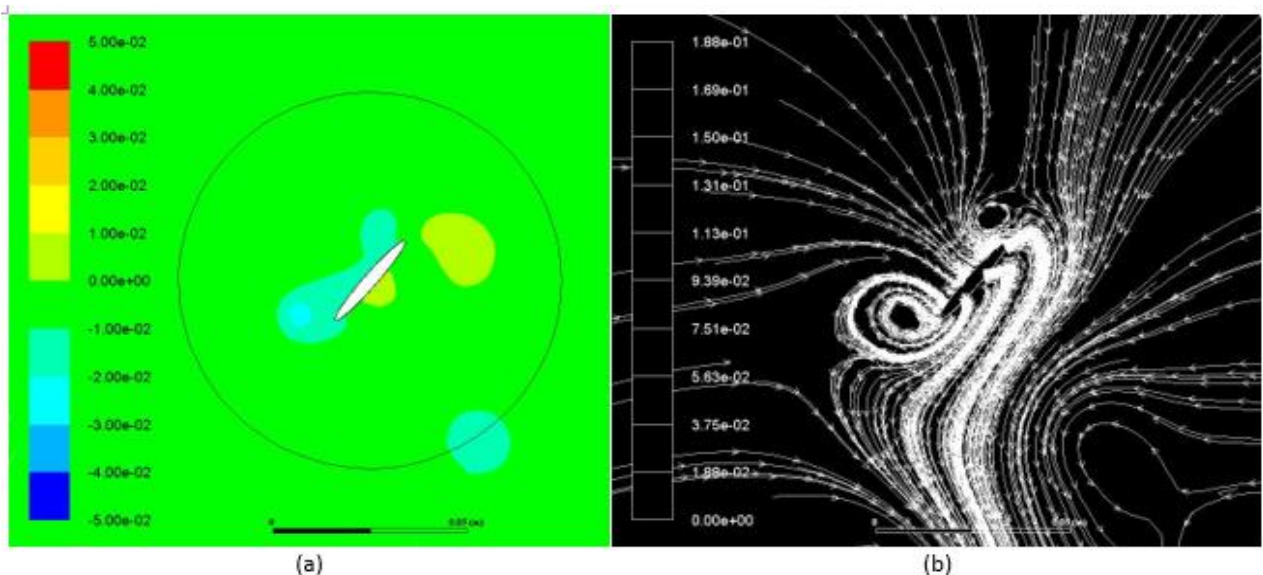


Fig. 5. Vortex dipoles at $t/T=0.9$; a) contour of static pressure and b) flow path-lines

5. Conclusions

A numerical analysis on the drag production of an elliptical airfoil at a low Re of 1000 has been performed. The force history shows that drag is produced mainly during the downstroke, while thrust is generated during the upstroke. It is found that the formation of counter-rotating vortices is closely related to the generation of thrust. The flow visualization shows that thrust is generated when counter-rotating vortices are attached to or shed by the airfoil. The time-averaged drag is 0.0470, which is low and represents the hovering mode of the airfoil. This low drag also implies that the insect can utilize asymmetrical strokes in normal hovering to minimize drag or produce thrust. In combination with the high lift ($\bar{C}_l = 0.6366$) produced during the development and shedding of counter-rotating vortices, the low drag results in a high lift-to-drag ratio of 13.5447. The high value of the lift-to-drag ratio shows the efficiency of bumblebee-inspired kinematics in normal-hovering mode.

References

- [1] Miao, J-M., and M-H. Ho. "Effect of flexure on aerodynamic propulsive efficiency of flapping flexible airfoil." *Journal of Fluids and Structures* 22, no. 3 (2006): 401-419. <https://doi.org/10.1016/j.jfluidstructs.2005.11.004>
- [2] Ashraf, M. A., J. Young, and J. C. S. Lai. "Reynolds number, thickness and camber effects on flapping airfoil propulsion." *Journal of Fluids and Structures* 27, no. 2 (2011): 145-160. <https://doi.org/10.1016/j.jfluidstructs.2010.11.010>
- [3] Xinyu, L. A. N. G., S. O. N. G. Bifeng, Y. A. N. G. Wenqing, and S. O. N. G. Wenping. "Aerodynamic performance of owl-like airfoil undergoing bio-inspired flapping kinematics." *Chinese Journal of Aeronautics* 34, no. 5 (2021): 239-252. <https://doi.org/10.1016/j.cja.2020.10.017>
- [4] Bao, Han, Wenqing Yang, Dongfu Ma, Wenping Song, and Bifeng Song. "Numerical simulation of flapping airfoil with alula." *International Journal of Micro Air Vehicles* 12 (2020): 1756829320977989. <https://doi.org/10.1177/1756829320977989>
- [5] Dickinson, Michael H., and Karl G. Götz. "The wake dynamics and flight forces of the fruit fly *Drosophila melanogaster*." *The Journal of experimental biology* 199, no. 9 (1996): 2085-2104. <https://doi.org/10.1038/35089071>
- [6] Birch, James M., and Michael H. Dickinson. "The influence of wing-wake interactions on the production of aerodynamic forces in flapping flight." *Journal of experimental biology* 206, no. 13 (2003): 2257-2272. <https://doi.org/10.1242/jeb.00381>
- [7] Yusoff, Hamid, Koay Mei Hyie, Halim Ghaffar, Aliff Farhan Mohd Yamin, Muhammad Ridzwan Ramli, Wan Mazlina Wan Mohamed, and Siti Nur Amalina Mohd Halidi. "The Evolution of Induced Drag of Multi-Winglets for Aerodynamic Performance of NACA23015." *Journal of Advanced Research in Fluid Mechanics and Thermal Sciences* 93, no. 2 (2022): 100-110. <https://doi.org/10.37934/arfmts.93.2.100110>
- [8] Yusoff, Hamid, Aliff Farhan Mohd Yamin, Siti Nur Amalina Mohd Halidi, Nor Suhada Abdullah, Halim Ghafar, Shafiq Suhaimi, Koay Mei Hyie, and Wan Mazlina Wan Mohamed. "The Optimisation of Aerodynamic Performance Enhancement of a Flapping Wing using Response Surface Methodology." *Journal of Advanced Research in Fluid Mechanics and Thermal Sciences* 91, no. 1 (2022): 69-82. <https://doi.org/10.37934/arfmts.91.1.6982>
- [9] Truong, Tri Quang, Vu Hoang Phan, Hoon Cheol Park, and Jin Hwan Ko. "Effect of wing twisting on aerodynamic performance of flapping wing system." *AIAA journal* 51, no. 7 (2013): 1612-1620. <https://doi.org/10.2514/1.J051831>
- [10] Eldredge, Jeff D., and Anya R. Jones. "Leading-edge vortices: mechanics and modeling." *Annual Review of Fluid Mechanics* 51 (2019): 75-104. <https://doi.org/10.1146/annurev-fluid-010518-040334>
- [11] Dickinson, Michael H., Fritz-Olaf Lehmann, and Sanjay P. Sane. "Wing rotation and the aerodynamic basis of insect flight." *Science* 284, no. 5422 (1999): 1954-1960. <https://doi.org/10.1126/science.284.5422.1954>
- [12] Byrne, David N., Stephen L. Buchmann, and Hayward G. Spangler. "Relationship between wing loading, wingbeat frequency and body mass in homopterous insects." *Journal of Experimental Biology* 135, no. 1 (1988): 9-23. <https://doi.org/10.1242/jeb.135.1.9>
- [13] Bomphrey, Richard James, Graham K. Taylor, and Adrian LR Thomas. "Smoke visualization of free-flying bumblebees indicates independent leading-edge vortices on each wing pair." In *Animal Locomotion*, pp. 249-259. Springer, Berlin, Heidelberg, 2010. https://doi.org/10.1007/978-3-642-11633-9_20

- [14] Tobing, S., J. Young, and J. C. S. Lai. "Effects of wing flexibility on bumblebee propulsion." *Journal of Fluids and Structures* 68 (2017): 141-157. <https://doi.org/10.1016/j.jfluidstructs.2016.10.005>
- [15] Heathcote, Sam, and Ismet Gursul. "Flexible flapping airfoil propulsion at low Reynolds numbers." *AIAA journal* 45, no. 5 (2007): 1066-1079. <https://doi.org/10.2514/6.2005-1405>
- [16] Yang, Tao, Mingjun Wei, and Hong Zhao. "Numerical study of flexible flapping wing propulsion." *AIAA journal* 48, no. 12 (2010): 2909-2915. <https://doi.org/10.2514/1.J050492>
- [17] Trizila, Pat, Chang-Kwon Kang, Hikaru Aono, Wei Shyy, and Miguel Visbal. "Low-Reynolds-number aerodynamics of a flapping rigid flat plate." *AIAA journal* 49, no. 4 (2011): 806-823. <https://doi.org/10.2514/1.J050827>
- [18] Wang, Z. Jane. "Two dimensional mechanism for insect hovering." *Physical review letters* 85, no. 10 (2000): 2216. <https://doi.org/10.1103/PhysRevLett.85.2216>
- [19] Poelma, C., W. B. Dickson, and M. H. Dickinson. "Time-resolved reconstruction of the full velocity field around a dynamically-scaled flapping wing." *Experiments in Fluids* 41, no. 2 (2006): 213-225. <https://doi.org/10.1007/s00348-006-0172-3>
- [20] Sun, Wei, Zhenghong Gao, Yiming Du, and Fang Xu. "Mechanism of unconventional aerodynamic characteristics of an elliptic airfoil." *Chinese Journal of Aeronautics* 28, no. 3 (2015): 687-694. <https://doi.org/10.1016/j.cja.2015.03.009>
- [21] Wang, Z. Jane. "The role of drag in insect hovering." *Journal of Experimental Biology* 207, no. 23 (2004): 4147-4155. <https://doi.org/10.1242/jeb.01239>
- [22] Tobing, S. "Lift generation of an elliptical airfoil at a reynolds number of 1000." *International Journal of Automotive and Mechanical Engineering* 16, no. 2 (2019): 6738-6752. <https://doi.org/10.15282/ijame.16.2.2019.20.0507>
- [23] Dudley, R., and C. P. Ellington. "Mechanics of forward flight in bumblebees: I. Kinematics and morphology." *Journal of Experimental Biology* 148, no. 1 (1990): 19-52. <https://doi.org/10.1242/jeb.148.1.19>
- [24] Engels, T., D. Kolomenskiy, Kai Schneider, F-O. Lehmann, and J. Sesterhenn. "Bumblebee flight in heavy turbulence." *Physical review letters* 116, no. 2 (2016): 028103. <https://doi.org/10.1103/PhysRevLett.116.028103>